

VIBRATIONALLY EXCITED HCN IN THE LUMINOUS INFRARED GALAXY NGC 4418

KAZUSHI SAKAMOTO¹, SUSANNE AALTO², AARON S. EVANS^{3,4}, MARTINA C. WIEDNER⁵, AND DAVID J. WILNER⁶

Accepted for publication in ApJ Letters

ABSTRACT

Infrared pumping and its effect on the excitation of HCN molecules can be important when using rotational lines of HCN to probe dense molecular gas in galaxy nuclei. We report the first extragalactic detection of (sub)millimeter rotational lines of vibrationally excited HCN, in the dust-enshrouded nucleus of the luminous infrared galaxy NGC 4418. We estimate the excitation temperature of $T_{\text{vib}} \approx 230$ K between the vibrational ground and excited ($v_2=1$) states. This excitation is most likely due to infrared radiation. At this high vibrational temperature the path through the $v_2=1$ state must have a strong impact on the rotational excitation in the vibrational ground level, although it may not be dominant for all rotational levels. Our observations also revealed nearly confusion limited lines of CO, HCN, HCO⁺, H¹³CN, HC¹⁵N, CS, N₂H⁺, and HC₃N at $\lambda \sim 1$ mm. Their relative intensities may also be affected by the infrared pumping.

Subject headings: galaxies: ISM — galaxies: active — galaxies: individual (NGC 4418)

1. INTRODUCTION

Hydrogen cyanide (HCN) is a major tracer of dense molecular gas in space. It decays fast in its rotational energy ladder, 300 times faster than carbon monoxide⁷, because of its large dipole moment. Rotationally excited HCN therefore suggests an excitation mechanism fast enough to counter the decay, such as frequent collisions with interstellar H₂ in dense molecular gas. HCN or any molecule with a large dipole moment, however, will not trace dense gas if there is another excitation mechanism that is faster than the H₂ collisions and independent of gas density. One such excitation path is through a vibrationally excited state, to which molecules can be pumped by infrared radiation (Carroll & Goldsmith 1981). This excitation is possible because a round trip of radiative transitions between the vibrational ground and excited states can change the rotational level J by 2. The first vibrationally excited state of HCN is its bending state ($v_2=1$) 1024 K above the ground (Fig. 1). Radiative excitation of HCN through this state has been observed around dusty evolved and young high-mass stars (Ziurys & Turner 1986). Meanwhile, despite the increasing number of extragalactic HCN observations, it has been controversial whether such radiative excitation is significant in extragalactic observations where the volume probed is much larger and having enough IR flux there more difficult (Aalto et al. 1995; Gao & Solomon 2004; García-Burillo et al. 2006; Krips et al. 2008; Graciá-Carpio et al. 2008). It was

found significant in a $10^{14} L_{\odot}$ quasar (Weiß et al. 2007; Riechers et al. 2010) but the quasar may be exceptional.

In this Letter, we report our detection of rotational transitions from vibrationally excited HCN in the luminous infrared galaxy NGC 4418. We analyze HCN excitation by measuring vibrational and rotational temperatures from the data. Our detection follows the detection of vibrationally excited HC₃N in the same galaxy by Costagliola & Aalto (2010). Related HCN lines are the $v_2=1 \leftarrow 0$ absorption at 14 μm in NGC 4418 and other galaxies (Lahuis et al. 2007) and the direct l -type transitions of vibrationally excited HCN in Arp 220 (Salter et al. 2008). NGC 4418 has a high luminosity and a compact and heavily dust shrouded nucleus ($L_{\text{IR}} = 10^{11.1} L_{\odot}$, size $\lesssim 100$ pc = $0''.6$; Dudley & Wynn-Williams 1997; Evans et al. 2003). Both an active galactic nucleus and a very young starburst have been proposed for the luminosity source (Spoon et al. 2001; Roussel et al. 2003).

2. SMA OBSERVATIONS

We observed the nucleus of NGC 4418 (R.A. = $12^{\text{h}}26^{\text{m}}54.62^{\text{s}}$, Dec. = $-00^{\circ}52'39.4''$; J2000) using the Submillimeter Array (SMA)⁸ in 2010 March and May in the subcompact and compact configurations, respectively. Receivers were tuned to around 350 GHz in March and 270 GHz in May for J=4–3 and 3–2 transitions of HCN and HCO⁺ as well as CO(3–2). Signals were separately recorded from upper and lower sidebands (USB and LSB), whose central frequencies are 12 GHz apart from each other. Each sideband is 4 GHz wide; we filled its central 30 MHz (~ 30 km s⁻¹) gap by interpolation. Spectral resolution was 1.625 and 3.25 MHz for our 270 and 350 GHz runs, respectively. The system gain, passband, and flux scale were calibrated using a nearby quasar 3C273 (which dimmed in May), quasars and planets, and Mars ($T_{\text{b } 270 \text{ GHz}}=190$ K and $T_{\text{b } 350 \text{ GHz}}=192$ K)

⁸ The Submillimeter Array is a joint project between the Smithsonian Astrophysical Observatory and the Academia Sinica Institute of Astronomy and Astrophysics, and is funded by the Smithsonian Institution and the Academia Sinica.

¹ Academia Sinica, Institute of Astronomy and Astrophysics, Taipei, Taiwan

² Onsala Space Observatory, Onsala, Sweden

³ Department of Astronomy, University of Virginia, Charlottesville, VA, USA

⁴ National Radio Astronomy Observatory, Charlottesville, VA, USA

⁵ Observatoire de Paris, Paris, France

⁶ Harvard-Smithsonian Center for Astrophysics, Cambridge, MA, USA

⁷ Molecular parameters in this Letter are from the Cologne Database of Molecular Spectroscopy (Müller et al. 2005) through Splatalogue (<http://www.splatalogue.net>) unless otherwise noted.

and Titan ($T_{\text{b } 270 \text{ GHz}}=77 \text{ K}$ for continuum), respectively.

We reduced the data using MIR and MIRIAD packages and made images with the natural weighting of visibilities at 30 km s^{-1} velocity resolution. The full width at half maximum of the synthesized beam was $5''.2$ for the 350 GHz data, which had projected baselines of 6–25 m, and $2''.6$ for the 270 GHz data (15–68 m). We did not subtract continuum in order to later determine the continuum and lines in the spectra. There are two calibration notes. First, we took the spectral index of 3C273 into account in our gain calibration in order to accurately scale the flux of our two sidebands. We used the spectral index $\alpha = -1.0$ (for $S_\nu \propto \nu^\alpha$), the mean of our March and May measurements. Second, we verified our passband calibration by setting aside a fraction of 3C273 data when determining passband shapes and by applying the same calibration to the galaxy and the 3C273 data. The flatness of the resulting test 3C273 spectra confirmed our calibration.

3. RESULTS

Strong continuum and line emission were detected at the nucleus of NGC 4418. No extended emission was detected off the nucleus except CO(3–2) that was marginally resolved. Any missing flux in our data is estimated to be less than our calibration error on the basis of the ratio of our flux to single-dish flux, 0.82 ± 0.19 for CO(3–2) (Yao et al. 2003) and 1.21 ± 0.19 for HCO⁺(4–3) (Aalto et al. in prep.)

Our spectra and emission parameters in the central kpc are presented in Fig. 2 and Table 1. The strongest line is CO(3–2) followed by HCN and HCO⁺ in both (4–3) and (3–2), CS(7–6), and N₂H⁺(3–2). We also identified H¹³CN and vibrationally excited HCN next to the CO and HCO⁺ lines, respectively. Although both are at about $+400 \text{ km s}^{-1}$ from the systemic velocity of the adjacent brighter lines, they cannot be a high-velocity gas because such a feature is absent in CO(2–1) (Fig. 3). This HCN is excited in its bending mode ($v_2=1$) and the line is one of the l -doublet ($l=1f$). The other line ($l=1e$) is only -38 km s^{-1} from the ground state HCN line and indistinguishable. At even lower levels, our data show line features that we attribute to HC¹⁵N and HC₃N. The data plausibly contain more lines, e.g., on both sides of HCN(3–2). Line density is high, and we are approaching the confusion limit.

The continuum, which we determined from ‘line free’ channels (details are in Table 1), has a spectral index of $\alpha = 2.7 \pm 0.5$ in our data excluding the 350 GHz USB. It is consistent with previous submillimeter measurements ($\alpha \sim 2.9$; Dunne et al. 2000; Yang & Phillips 2007). The 350 GHz USB continuum is an outlier with $\alpha = 6.25 \pm 0.84$ between the 350 GHz sidebands (cf. $\alpha = 2.40 \pm 1.04$ between our 270 GHz sidebands). The 350 GHz ‘line free’ channels may thus contain blended lines. The contamination would be 23 mJy (i.e., 12%) if we scale the LSB continuum with $\alpha = 3$. This possible error is not included in Table 1 and it would affect weak lines more.

4. HCN EXCITATION

We obtained the following HCN excitation temperatures among (v_2^l, J)=($1^{1f}, 4$), ($1^{1f}, 3$), and ($0, 4$) states under the assumptions described below: $T_{\text{ex}}(1^{1f}, 4; 1^{1f}, 3)=31 \pm 13 \text{ K}$, $T_{\text{ex}}(1^{1f}, 4; 0, 4)=227 \pm 18 \text{ K}$, and

$T_{\text{ex}}(1^{1f}, 3; 0, 4)=254 \pm 24 \text{ K}$. The first one is a rotational excitation temperature T_{rot} and the second is a vibrational excitation temperature T_{vib} . We needed opacity correction to the HCN(4–3) flux for these excitation temperatures because the line is almost certainly saturated considering its low flux ratio, 3, to H¹³CN(4–3). We adopted $3000 \pm 1000 \text{ Jy km s}^{-1}$ as the opacity-corrected HCN(4–3) flux on the basis of H¹³CN(4–3) and HC¹⁵N(4–3) fluxes and the abundance ratios [¹²C/¹³C] ≈ 50 and [¹⁴N/¹⁵N] ≈ 300 (Wilson 1999, Milky Way inner disk values). We also assumed that the vibrationally excited lines are optically thin, because if they were thick they would be as bright as the $v_2=0$ lines. Another assumption here and in the T_{ex} calculation above is that all HCN lines arise from the same volume.

The vibrational excitation is most likely due to infrared radiation rather than collision for our T_{vib} and T_{rot} . This is because collisional excitation would make T_{rot} at $v_2=1$ equal to T_{vib} . If the excitation were due to H₂ collision at $\sim 200 \text{ K}$ the gas needs to be at or above the critical density for HCN $v_2=1$, which is $n_{\text{H}_2} \sim 5 \times 10^{11} \text{ cm}^{-3}$ (Ziurys & Turner 1986). Radiative excitation is energetically possible. Each rotational state J at the vibrational ground level has associated infrared absorption lines in the P, Q, and R branches. The absorption lines supply energy to the HCN($J, J-1$) emission line, and weaker rotational lines at $v_2=1$, in the limit of radiation-dominated excitation. Thus, an energy requirement for IR-pumping is

$$\sum_{i=P,Q,R} f_i S_{\text{IR}}/\lambda_{\text{IR}} \gtrsim S_{\text{rot}}/\lambda_{\text{rot}}, \quad (1)$$

assuming that all the lines have the same velocity width. Here, S_{IR} is the continuum flux density around the absorption wavelength λ_{IR} , f_i is the fractional absorption depth, and S_{rot} is the mean flux density of the rotational emission line at the wavelength λ_{rot} . Parameters for our case are $\lambda_{\text{IR}}=14 \mu\text{m}$, $S_{14\mu\text{m}}=2.34 \text{ Jy}$ and $f_Q \sim 0.3$ (Lahuis et al. 2007), and $\lambda_{\text{rot}}=850 \mu\text{m}$ and $S_{\text{rot}} \lesssim 1 \text{ Jy}$ for $J=4$. The condition of Eq. (1) is satisfied with a wide margin; the excess energy heats gas through collision. In this radiative excitation, the observed T_{vib} indicates that the brightness temperature of the excitation source seen from the gas must be $\geq 200 \text{ K}$ at $14 \mu\text{m}$.

The vibrational excitation significantly affects rotational excitation in the vibrational ground level. We see this in a model with two vibrational levels, $v=0$ and 1, whose energy gap is T_0 in temperature. Each vibrational level has rotational sub-levels labeled with J . For a molecule at (v, J)=($0, J$) there exist approximately $e^{-T_0/T_{\text{vib}}}$ molecules at $v=1$ that will spontaneously decay to the ($0, J$) state. Thus the rate of spontaneous transition to ($0, J$) from $v=1$ is $e^{-T_0/T_{\text{vib}}} A_{\text{vib}}$, and radiative excitation of the J level at $v=0$ through $v=1$ needs

$$e^{-T_0/T_{\text{vib}}} A_{\text{vib}} \geq A_{\text{rot } J} \Leftrightarrow T_{\text{vib}} \geq T_0 / \ln \frac{A_{\text{vib}}}{A_{\text{rot } J}}, \quad (2)$$

where A_{vib} and A_{rot} are the Einstein A coefficients for the vibrational and rotational transitions, respectively. This is equivalent to Equation (6) of Carroll & Goldsmith (1981) but is more useful when T_{vib} is available. Similarly, the radiative excitation through $v=1$ exceeds col-

lisional (de)excitation among $v=0$ rotational levels when

$$e^{-T_0/T_{\text{vib}}} A_{\text{vib}} \geq n_{\text{col}} \gamma_{J,J-1}, \quad (3)$$

where n_{col} is the number density of the main collision partner and $\gamma_{J,J-1}$ is the collisional rate coefficient. In other words, radiative pumping to $v=1$ is equivalent to a gas density $e^{-T_0/T_{\text{vib}}} A_{\text{vib}}/\gamma_{J,J-1}$ in terms of the rotational excitation around J at $v=0$. Parameters for HCN are $T_0=1024$ K and $A_{\text{vib}}=3.7$ s $^{-1}$ for the bending mode (Ziurys & Turner 1986) and $\gamma_{J,J-1} \approx 1 \times 10^{-11}$ cm 3 s $^{-1}$ for HCN–H $_2$ collisions at $J \leq 10$ and gas kinetic temperatures 30–300 K (Dumouchel et al. 2010). For the observed T_{vib} of 227 K, the rate $e^{-T_0/T_{\text{vib}}} A_{\text{vib}}$ is 0.04 s $^{-1}$ and 20 times larger (faster) than $A_{\text{rot } J=4-3}$. The minimum T_{vib} to satisfy Eq. (2) is 86, 137, and 218 K for $J=1, 4,$ and $10,$ respectively. Thus the observed T_{vib} satisfies Eq. (2) for J s up to about 10. The IR-pumping through $v_2=1$ matches $n_{\text{H}_2} \sim 10^9$ cm $^{-3}$ for our T_{vib} according to Eq. (3), although this is somewhat overestimated because collisional transitions are not limited to $|\Delta J| = 1$ and half of the vibrational transitions are in the Q branch where $\Delta J = 0$.

The relatively low rotational temperature $T_{\text{rot}}(v_2=1^f; J \sim 4) = 31 \pm 13$ K probably suggests that the system is not in local thermodynamic equilibrium (LTE). A caution here is that T_{rot} may be higher and even comparable to T_{vib} depending on the uncertain 355 GHz continuum mentioned in §3; T_{rot} would be 59^{+125}_{-27} K if we adopt the lower continuum level estimated from the LSB. A possible reason for the lower rotational temperature than T_{vib} is that rotational excitation at low J ($\lesssim 5$) is strongly affected by collision and (sub)millimeter radiation; note that HCN(4–3) is optically thick. The T_{rot} at $v_2=1$ may be relatively low accordingly. Rotational temperature can be higher in higher J since collisional excitation in <100 K gas gives way there to IR-pumping as the main excitation mechanism. This may explain the HCN (rotational) temperature of 300 K ($\pm 30\%$) that Lahuis et al. (2007) estimated from the Q-branch absorption profile under LTE assumption, because high J population broadens the profile.

For comparison, we analyzed the $v = 0$ HCN lines alone using the large-velocity-gradient model via RADEX (van der Tak et al. 2007; Schöier et al. 2005) and found two types of solutions. We used for this the abundance ratios mentioned above and HCN(1–0) data from Imanishi et al. (2004). One solution has thermalized HCN at $J=4$, $N_{\text{HCN}}/\Delta V \approx 10^{14.7}$ cm $^{-2}$ (km s $^{-1}$) $^{-1}$, $T_{\text{kin}} \approx 40$ K, and $n_{\text{H}_2} \geq 10^{7.5}$ cm $^{-3}$. Another has subthermal excitation at $J=4$, moderate opacity of H 13 CN, and such parameters as $N_{\text{HCN}}/\Delta V \approx 10^{15}$ cm $^{-2}$ (km s $^{-1}$) $^{-1}$, $T_{\text{kin}} \geq 30$ K, and $n_{\text{H}_2} \approx 10^6$ cm $^{-3}$. These temperatures are consistent with our T_{rot} at $v_2=1$ and the high column densities are in accord with the deep obscuration toward the nucleus. However, these solutions cannot explain the observed HCN $v_2=1$ lines.

To summarize, the vibrationally excited HCN is most likely IR pumped, and the observed degree of vibrational excitation suggests strong influence of the excitation path through $v_2=1$ to the rotational excitation in the ground state although it may not dominate low- J excitation. Properties of (dense) molecular gas in NGC 4418 cannot

be studied through HCN ignoring the IR-pumping. In further study, one needs to reexamine our simplistic assumptions that the emitting regions of $v_2=0$ and 1 lines are cospatial and have a single characteristic temperature and density. In reality, gas density must be diverse, and there must be low density gas where HCN is excited only under the IR-pumping. Thus the total flux of any HCN $v=0$ line should be enhanced at least for that component. Another improvement in modeling would be to include atomic hydrogen and electrons as collision partners (Scoville et al. 1980; Faure et al. 2007).

5. OTHER LINES AND OTHER GALAXIES

HC $_3$ N is detected in its vibrational ground and excited states though some transitions are marginal or blended with other lines. Its population diagram in Fig. 4 shows that the measured line fluxes are consistent with those of other transitions detected by Costagliola & Aalto (2010). The diagram indicates overall excitation temperatures in the range of ~ 100 –300 K, except for the $E/k < 100$ K levels where Costagliola & Aalto (2010) estimated $T_{\text{rot}}=29$ K for $v=0$. They also obtained $T_{\text{vib}} \sim 500$ K. These temperatures are compatible with our HCN excitation temperatures.

The HCN to HCO $^+$ ratio of the mean brightness temperatures is 1.65 ± 0.07 for $J=4-3$ and 1.61 ± 0.08 for $J=3-2$ on the assumption of the same emitting volume; it is 1.9 for $J=1-0$ (Imanishi et al. 2004). Brighter HCN than HCO $^+$ in some Seyfert galaxies and in this galaxy has been proposed to be a result of or evidence for chemistry driven by X-ray radiation from active nucleus (Kohno et al. 2001; Imanishi et al. 2004) although there have been different views (e.g., Lahuis et al. 2007; Baan et al. 2010). It is conceivable at least for objects as deeply embedded as the nucleus of NGC 4418 that the IR-pumping also affects this ratio. The minimum brightness temperature of the infrared source needed for the radiative pumping of $J=1$ is given by Eq. (2) as $T_{\text{b}}^{\text{min}} = T_0/\ln(A_{\text{vib}}/A_{\text{rot } 1-0})$ because vibrational temperature is at or below the source brightness temperature at the wavelength of the vibrational transition. This minimum temperature is 86 K at 14 μm for HCN and 156, 115, 107, 80, and 33 K at 4.6, 7.8, 12, 15, and 45 μm for CO, CS, HCO $^+$, N $_2$ H $^+$, and HC $_3$ N, respectively (Chandra et al. 1996, 1995; Mauclair et al. 1995; Heninger et al. 2003, for A_{vib}). We note that HCO $^+$ needs higher T_{b} than HCN for IR-pumping and that vibrationally excited HCO $^+$ (3–2) is not detected at an expected frequency of 266.8 GHz (see Fig. 2). IR-pumping may therefore play a role in NGC 4418 for the high HCN-to-HCO $^+$ ratio and maybe also for HCN-to-CO ratio and the bright N $_2$ H $^+$. Its synergy with chemistry in hot galaxy nuclei (e.g., Harada et al. 2010) needs further study.

We searched published spectra for the HCN($v_2 = 1^f$) rotational lines at +400 km s $^{-1}$ of HCO $^+$ ($v = 0$) to assess the prevalence of the HCN infrared pumping. We found no convincing case though a possible sign is at NGC 6240 nucleus in Wilson et al. (2008). The limitations are sensitivity, spectral baseline, and blending with the brighter HCO $^+$ lines. The lines must be as narrow as in NGC 4418 for unambiguous detection.

6. CONCLUDING REMARKS

We evaluated the effect of infrared pumping to the rotational excitation of HCN using vibrational and rotational temperatures. The vibrational temperature became measurable with our detection of rotational lines from vibrationally excited HCN. The high T_{vib} in NGC 4418 suggests that HCN is IR pumped and cannot simply trace dense gas in the nucleus. Other molecules should also be subject to the pumping in different degrees according to their energy structures, A coefficients, spatial distributions, and the spectrum of the radiation field. Observations of T_{vib} in various molecules and galaxies will tell us the overall significance of IR-pumping in extragalactic observations. Regarding NGC 4418, our high T_{vib} of HCN agrees with earlier studies to suggest a ≥ 200 K excitation source in the nucleus. The (sub)millimeter lines from vibrationally excited HCN are our new tool to probe hot molecular gas close to the nuclear heat source.

We thank Daniel Espada for the CO(2–1) spectrum, Mark Gurwell for advice on flux calibration, the SMA operation team for the service observations, and the referee for helpful comments. This research extensively used the NASA/IPAC Extragalactic Database, NASA’s Astrophysics Data System, the Cologne Database of Molecular Spectroscopy, and the Splatalogue database. This work was supported by the grant 99-2112-M-001-011-MY3 from the National Science Council of Taiwan.

Facilities: SMA

REFERENCES

- Aalto, S., Booth, R. S., Black, J. H., & Johansson, L. E. B. 1995, *A&A*, 300, 369
- Baan, W. A., Loenen, A. F., & Spaans, M. 2010, *A&A*, 516, A40
- Carroll, T. J., & Goldsmith, P. F. 1981, *ApJ*, 245, 891
- Chandra, S., Kegel, W. H., Le Roy, R. J., & Hertenstein, T. 1995, *A&AS*, 114, 175
- Chandra, S., Maheshwari, V. U., & Sharma, A. K. 1996, *A&AS*, 117, 557
- Costagliola, F., & Aalto, S. 2010, *A&A*, 515, A71
- Dudley, C. C., & Wynn-Williams, C. G. 1997, *ApJ*, 488, 720
- Dumouchel, F., Faure, A., & Lique, F. 2010, *MNRAS*, 406, 2488
- Dunne, L., Eales, S., Edmunds, M., Ivison, R., Alexander, P., & Clements, D. L. 2000, *MNRAS*, 315, 115
- Espada, D., et al. 2010, arXiv:1010.3428
- Evans, A. S., et al. 2003, *AJ*, 125, 2341
- Faure, A., Varambhia, H. N., Stoecklin, T., & Tennyson, J. 2007, *MNRAS*, 382, 840
- Gao, Y., & Solomon, P. M. 2004, *ApJS*, 152, 63
- García-Burillo, S., et al. 2006, *ApJ*, 645, L17
- Graciá-Carpio, J., García-Burillo, S., Planesas, P., Fuente, A., & Usero, A. 2008, *A&A*, 479, 703
- Harada, N., Herbst, E., & Wakelam, V. 2010, *ApJ*, 721, 1570
- Heninger, M., Lauvergnat, D., Lemaire, J., Boissel, P., Mauclaire, G., & Marx, R. 2003, *Int. J. Mass Spectrom.*, 223, 669
- Imanishi, M., Nakanishi, K., Kuno, N., & Kohno, K. 2004, *AJ*, 128, 2037
- Kohno, K., et al. 2001, *The Central Kiloparsec of Starbursts and AGN: The La Palma Connection*, ASP. Conf. Ser., 249, 672
- Krips, M., Neri, R., García-Burillo, S., Martín, S., Combes, F., Graciá-Carpio, J., & Eckart, A. 2008, *ApJ*, 677, 262
- Lahuis, F. et al. 2007, *ApJ*, 659, 296
- Mauclaire, G., Lemaire, J., Heninger, M., Fenistein, S., Parent, D. C., & Marx, R. 1995, *Int. J. Mass Spectrom. Ion Process.*, 149/150, 487
- Müller, H. S. P., Schlöder, F., Stutzki, J., & Winnewisser, G. 2005, *J. Mol. Struct.*, 742, 215
- Riechers, D. A., Weiss, A., Walter, F., & Wagg, J. 2010, *ApJ*, 725, 1032
- Roussel, H., Helou, G., Beck, R., Condon, J. J., Bosma, A., Matthews, K., & Jarrett, T. H. 2003, *ApJ*, 593, 733
- Salter, C. J., Ghosh, T., Catinella, B., Lebron, M., Lerner, M. S., Minchin, R., & Momjian, E. 2008, *AJ*, 136, 389
- Schöier, F. L., van der Tak, F. F. S., van Dishoeck, E. F., & Black, J. H. 2005, *A&A*, 432, 369
- Scoville, N. Z., Krotkov, R., & Wang, D. 1980, *ApJ*, 240, 929
- Spoon, H. W. W., Keane, J. V., Tielens, A. G. G. M., Lutz, D., & Moorwood, A. F. M. 2001, *A&A*, 365, L353
- van der Tak, F. F. S., Black, J. H., Schöier, F. L., Jansen, D. J., & van Dishoeck, E. F. 2007, *A&A*, 468, 627
- Weiß, A., Downes, D., Neri, R., Walter, F., Henkel, C., Wilner, D. J., Wagg, J., & Wiklind, T. 2007, *A&A*, 467, 955
- Wilson, C. D., et al. 2008, *ApJS*, 178, 189
- Wilson, T. L., 1999, *Rep. Prog. Phys.*, 62, 143
- Yang, M., & Phillips, T. 2007, *ApJ*, 662, 284
- Yao, L., Seaquist, E. R., Kuno, N., & Dunne, L. 2003, *ApJ*, 588, 771
- Ziurys, L. M., & Turner, B. E. 1986, *ApJ*, 300, L19

Table 1
Emission Properties of NGC 4418

Emission	f_{rest} [GHz]	E_u/k [K]	$F(\text{line}), S_\lambda$ [Jy km s ⁻¹ , mJy]	σ_{th}	σ_{tot}	note
(1)	(2)	(3)	(4)	(5)	(6)	(7)
HCO ⁺ (J=4-3)	356.734	42.8	82	3	9	
HCN($v_2=1^{1f}, J=4-3$)	356.256	1067.1	30	3	4	
HC ₃ N($v_7=1^{1e}, J=39-38$)	355.566	662.2	6	3	3	(a)
HC ₃ N(J=39-38)	354.697	340.5	25	...	10	(b)
HCN(J=4-3)	354.505	42.5	133	3	14	(c)
CO(J=3-2)	345.786	33.2	746	3	75	(d)
CO(J=3-2), 10''	345.796	33.2	782	3	78	(d)
H ¹³ CN(J=4-3)	345.340	41.4	41	4	5	(e)
HC ¹⁵ N(J=4-3)	344.200	41.3	11	3	3	
CS(J=7-6)	342.883	65.8	63	3	7	
N ₂ H ⁺ (J=3-2)	279.512	26.8	25	2	3	
HCO ⁺ (J=3-2)	267.558	25.7	59	2	6	
HCN($v_2=1^{1f}, J=3-2$)	267.199	1050.0	16	2	3	
HCN(J=3-2)	265.886	25.5	94	2	10	
HC ₃ N($v_7=1^{1f}, J=29-28$)	264.817	511.5	11	2	3	(f)
0.85 mm continuum	210	5	22	(g)
0.88 mm continuum	169	3	17	(g)
1.08 mm continuum	96	2	10	(g)
1.13 mm continuum	86	3	9	(h)

Note. — (2) Line frequency. (3) Upper level energy. (4) Line flux in Jy km s⁻¹ and continuum flux density in mJy in the central 6'' (1 kpc). Line fluxes are integrated over 1900–2300 km s⁻¹ unless otherwise noted and are continuum subtracted. No correction is made for missing flux. CO(3-2) flux is also given for the central 10''. No other emission was resolved by the 6'' beam. (5) Thermal error of (4). For lines, this includes thermal noise of continuum propagated through continuum subtraction. (6) Total error of (4) including σ_{th} and 10% error of flux calibration. (a) Marginal detection with possible blending with weaker lines. (b) Large uncertainty due to line blending. (c) No subtraction is made for the blended HC₃N(39-38). (d) There is likely contamination by HC₃N(J=38-37) at $f_{\text{rest}}=345.609$ GHz (Costagliola & Aalto 2010). (e) This line is blended with CO(3-2) and likely with HC₃N(38-37). Its flux is obtained by doubling the line flux in 2100–2300 km s⁻¹ assuming a symmetric profile. (f) Flux from 1900–2197 km s⁻¹. (g) Continuum flux densities are measured outside the 1900–2300 km s⁻¹ velocity ranges of the lines marked in Fig. 2. Also excluded for 0.85 mm continuum are HCN(4-3) velocities of 2300–2320 km s⁻¹. (h) Flux density is measured at the HCO⁺(3-2) velocities below 1900 km s⁻¹.

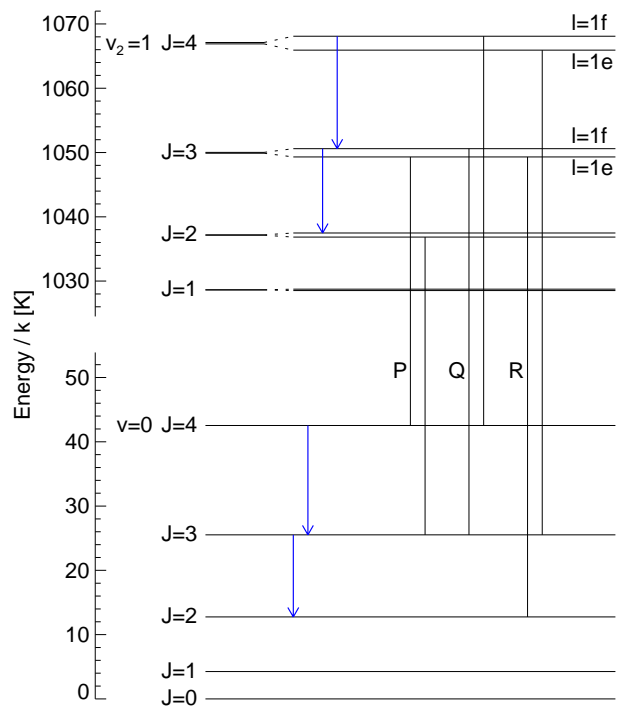


Figure 1. HCN energy level diagram, with l -doublets magnified 10 times on the right. Blue arrows are the rotational transitions that we detected. Allowed vibrational transitions are $v_2 = 0 \leftrightarrow 1^1f$, $\Delta J = 0$ (Q branch) and $v_2 = 0 \leftrightarrow 1^1e$, $\Delta J = \pm 1$ (P and R branches); some of them are plotted.

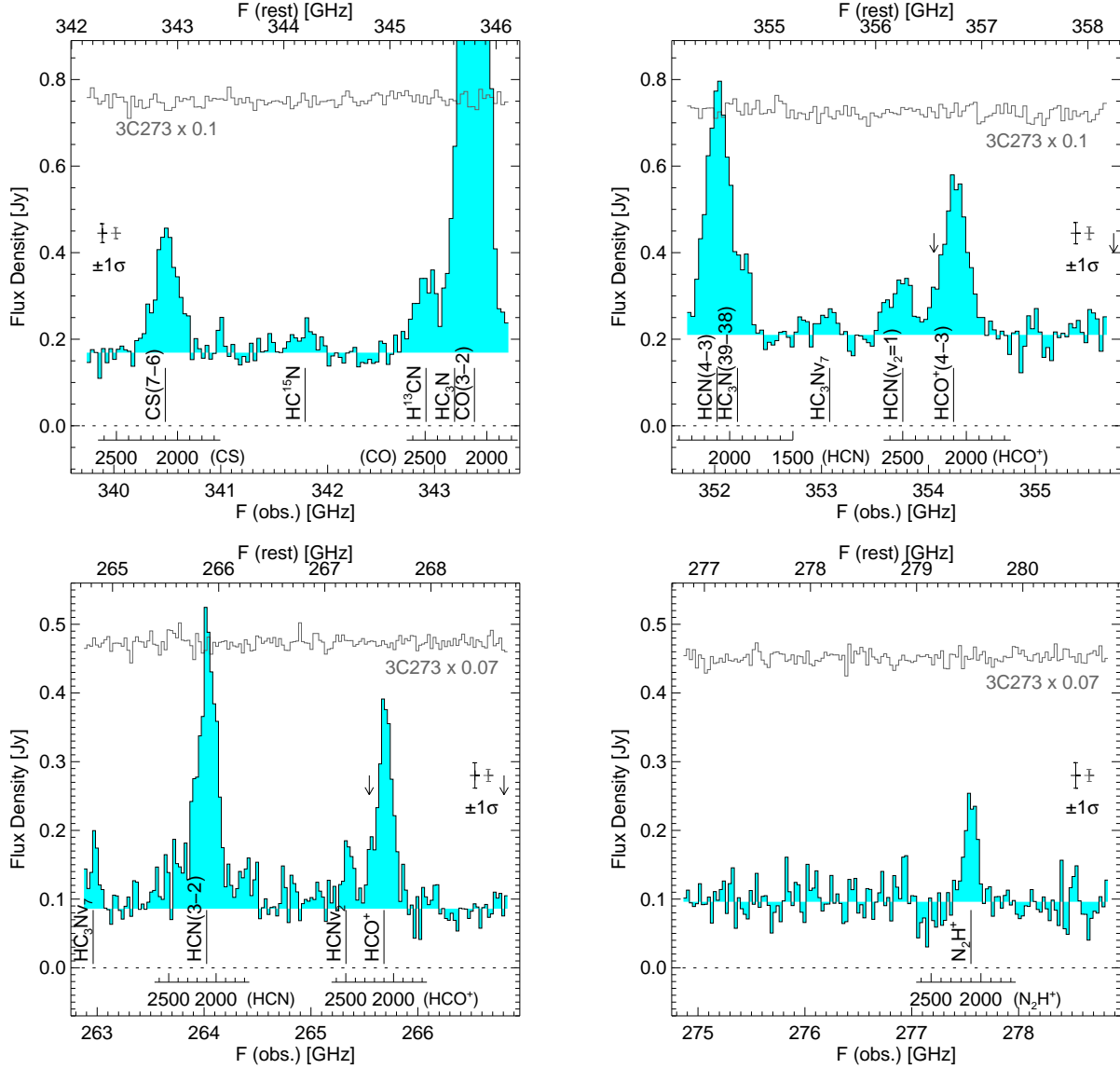


Figure 2. Spectra of the central 6'' (1 kpc) of NGC 4418. Major lines are marked at the redshift of the galaxy (2100 km s⁻¹). Full line names are in Table 1. Velocity axes are given for strong lines. Baselines of the shaded parts of the spectra are the continuum levels. Pairs of arrows in the top-right and bottom-left panels mark the frequencies of the HCO⁺(v₂=1) doublet. Scaled spectra of 3C273 from the same observations are also plotted to verify passband calibration.

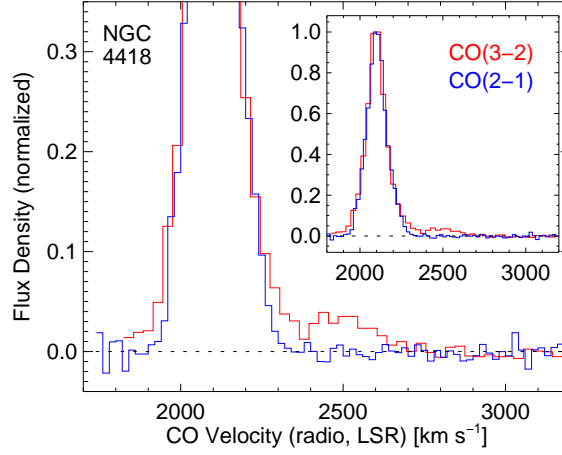


Figure 3. Comparison of CO(3-2) and CO(2-1) spectra, showing that CO(2-1) has no emission (i.e., no high-velocity gas) at 2500 ($=V_{\text{sys}} + 400$) km s^{-1} . The continuum-subtracted spectra of CO(3-2) and (2-1) are from the data in Fig. 2 and 3'' resolution SMA observations (Espada et al. 2010), respectively.

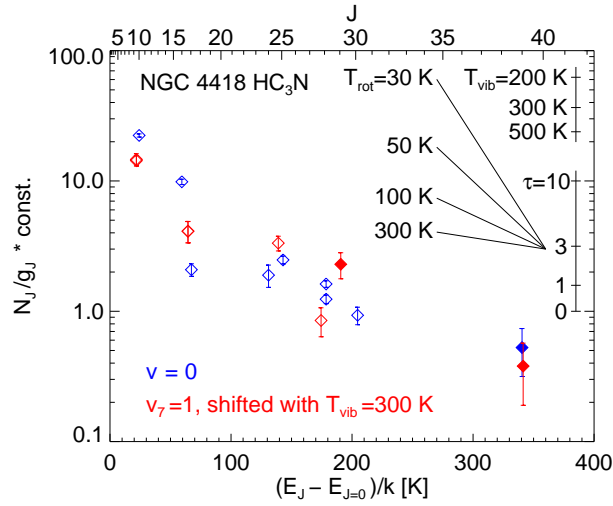


Figure 4. Population diagram of HC_3N . The lower and upper abscissae are rotational energy measured from the rotational ground level of each vibrational state and rotational quantum number J , respectively. The ordinate is population divided by the degree of degeneracy, $N_{J,v,l}/g_J$, in arbitrary unit. Open data points are from Costagliola & Aalto (2010) and filled ones are from our observations. Error bars are $\pm 1\sigma$. No correction is made for optical depth, but shifts needed for the correction are shown in the right side of the plot. The data for $v_7 = 1$ lines (red) are shifted against those for the vibrational ground ones (blue) using a vibrational temperature $T_{\text{vib}} = 300$ K. (The $v_7=1$ state is 321 K above $v=0$.) Shifts for other T_{vib} are shown in the top-right corner. To its left are the slopes of rotational population for various rotational temperatures.